

Journal of Materials Chemistry A

Accepted Manuscript



This is an *Accepted Manuscript*, which has been through the Royal Society of Chemistry peer review process and has been accepted for publication.

Accepted Manuscripts are published online shortly after acceptance, before technical editing, formatting and proof reading. Using this free service, authors can make their results available to the community, in citable form, before we publish the edited article. We will replace this *Accepted Manuscript* with the edited and formatted *Advance Article* as soon as it is available.

You can find more information about *Accepted Manuscripts* in the [Information for Authors](#).

Please note that technical editing may introduce minor changes to the text and/or graphics, which may alter content. The journal's standard [Terms & Conditions](#) and the [Ethical guidelines](#) still apply. In no event shall the Royal Society of Chemistry be held responsible for any errors or omissions in this *Accepted Manuscript* or any consequences arising from the use of any information it contains.

Amphiphilic superabsorbent cellulose nanofibril aerogels

Feng Jiang, and You-Lo Hsieh*

Ultra-light (1.7 to 8.1 mg/cm³) and ultra-porous (99.5 to 99.9%) aerogels have been assembled from cellulose nanofibrils (CNFs) that were defibrillated from rice straw cellulose at 96.8% yield. The as-prepared aerogels amphiphilic super-absorbents, absorbing 210 and 375 times of water and chloroform, respectively, far superior to any previously reported cellulose aerogels. Vapor deposition with triethoxyl(octyl) silane turned the amphiphilic aerogel more hydrophobic and oleophilic, capable of absorbing 139-356 times of non-polar hydrocarbons, polar aprotic solvents and oils, surpassing all previously reported polymeric, cellulosic and carbonaceous aerogels by 2 to nearly 20 times. These aerogels are excellent amphiphilic super-absorbents for selective oil removal and recovery.

Organic pollutants from industrial wastewater and oil spills are of increasing environmental and ecological concerns and have been remediated by various approaches including applying booms, skimmers, absorbents, in-situ burning, hydrocarbon-degrading microorganisms, dispersants and solidifiers.¹⁻⁴ Removing pollutants by low cost and highly absorbent materials is easy to implement and attractive as it does not generate by-products that may cause further concerns. Among the numerous oil absorbents, most inorganic absorbents, such as expanded perlite,⁵ inorganic minerals,⁶ clays,⁷ as well as polyacrylonitrile based activated carbon fibers,⁸ polypropylene nonwovens,^{5,9} and microporous polydivinylbenzene and porphyrin based sponges,¹⁰⁻¹² have low absorption capacities, typically less than 20 times by weight. These absorbents also suffer from drawbacks such as insufficient buoyance of the inorganics and very slow biodegradability of the synthetics.

Lignocellulosic materials are attractive because of their high absorption capacities as well as renewability and biodegradability. Cotton fibers¹³ and chopped rice straw¹⁴ were made hydrophobic by acylation to demonstrate 20-30 g/g oil absorption capacities; while the naturally waxy hollow milkweed floss¹⁵ and kapok fibers¹⁶ showed higher ca. 50 g/g absorption capacity. Nanocellulose aerogels from freeze-drying of aqueous nanocellulose suspension¹⁷,¹⁸ were modified to be hydrophobic and oleophilic with TiO₂ coating^{19,20} or vapor phase silanization,²¹ serving as absorbents¹⁹⁻²¹ for linear and cyclic alkanes and chloroform at up to 40 g/g absorption capacities,^{20,21} however, no higher than absorbents from previously mentioned natural fibers.

With the advent of carbon- and bio-based nanofibers fabrication and controlled assembly,²²⁻²⁶ super lightweight carbon-based aerogels, super hydrophobic and oleophilic absorbents including those from carbon nanotube (CNT),²⁷ graphene,²⁸⁻³⁰ CNT/graphene composite,³¹ carbonized bacterial cellulose (BC)³² or carbonaceous

nanofibers,³³ have been reported to show much higher solvent and oil absorbency ranging from 100-913 g/g, more than one order of magnitude higher than other absorbents. These carbon-based aerogels require complicated and energy-consuming processes to fabricate, thus are expensive.

Although nanocellulose aerogels have been made hydrophobic to absorb oils,^{17, 20, 21} their oil absorbency was low (around 40 g/g) and densities high (over 10 mg/cm³). Considering the nano-scale lateral dimensions of nanocellulose, the potential to generate porous structures with ultra-low density (less than 5 mg/cm³) and exceptionally high porosity (over 99%), thus absorbency, is ample and could be further exploited. Furthermore, with both hydrophilic hydroxyls and hydrophobic pyranose rings, cellulose chain is amphiphilic.^{34, 35} However, the amphiphilic nature of CNFs and assembled CNF aerogels are yet to be explored. Amphiphilicity of CNF aerogels would allow uptake of both polar and nonpolar liquids, in contrast to the hydrophobic carbon-based aerogels and the hydrophilic inorganic oxide aerogels. Additionally, the ample surface hydroxyls allow modification to tune the amphiphilicity toward greater hydrophobicity. Chemical vapor deposition of organosilane has been demonstrated a facile process for tuning the hydrophobicity of hydrophilic surfaces.^{20, 21, 36}

Herein, we report a facile and greener route to optimize the pore sizes and volumes of 3D interconnected ultra-porous aerogels by controlled assembly of cellulose nanofibrils (CNFs) from rice straw cellulose. The as-prepared aerogels have densities as low as 1.7 mg/cm³ and porosities up to 99.9%. The CNF aerogels are amphiphilic, absorbing 210 and 375 times of water and chloroform, respectively, far superior to any previously reported cellulose aerogels.^{20, 37, 38} Further modification with triethoxyl(octyl) silane turns some hydrophilic portions of the amphiphilic aerogel to hydrophobic and oleophilic, capable of absorbing 139-356 times of non-polar hydrocarbons, polar aprotic solvents and oils, surpassing all previously reported polymeric, cellulosic and carbonaceous aerogels by 2 to nearly 20 times.

Cellulose, isolated from rice straw at 36% yield,³⁹ was defibrillated by coupled (2,2,6,6-tetramethylpyridine-1-oxyl) TEMPO oxidation and mechanical blending to 1-2 nm wide and up to 1 μ m long CNFs (**Figure 1a**) at 96.8% yield (Description in Supporting Information).⁴⁰ Dilute aqueous CNF suspensions (0.1 to 0.6 wt%) were frozen at -20 °C for 15 h then slowly freeze-dried (-50 °C, 0.05 mbar, 2 days) to produce xCNF aerogels (**Figure S1**, Supporting Information), where x designates CNF concentration. These CNF aerogels have ultra-low densities from 1.7 to 8.1 mg/cm³ and ultra-high porosities from 99.5 to 99.9%, increasing and decreasing with increasing CNF concentrations, respectively, at high linearity with R² of 0.9922 (**Figure 1b**). All aerogels retain cellulose I β crystalline

structure with the characteristic XRD peaks at $2\theta=14.7^\circ$, 16.8° and 22.7° and 61.5% crystallinity (Figure 1c). The 1.7 mg/cm^3 density of 0.1CNF aerogel is significantly lower than those reported ($5\text{--}10 \text{ mg/cm}^3$) for cellulose aerogels^{18,41} and, most remarkably, even lower than aerogels fabricated from silica ($2\text{--}3 \text{ mg/cm}^3$),⁴² CNT (4 mg/cm^3),⁴³ and graphene (2.1 mg/cm^3).²⁸ A tubular shaped 0.2CNF aerogel with 1.2 cm diameter and 2.8 cm length weighs only 8.3 mg (Figure S2) and can be supported by a dandelion without deforming the fluffy seed heads (Figure 1d) as well as “fly” toward a plastic tube by static electricity (Movie S1).

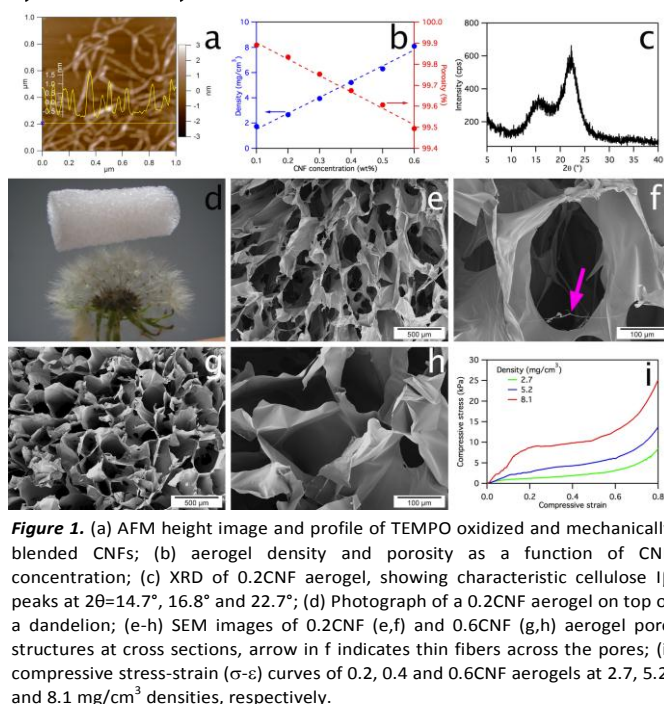
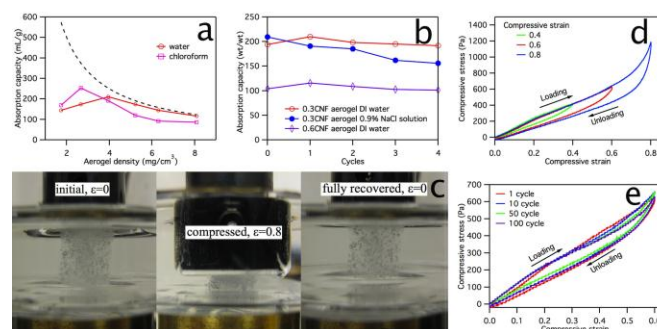


Figure 1. (a) AFM height image and profile of TEMPO oxidized and mechanically blended CNFs; (b) aerogel density and porosity as a function of CNF concentration; (c) XRD of 0.2CNF aerogel, showing characteristic cellulose I β peaks at $2\theta=14.7^\circ$, 16.8° and 22.7° ; (d) Photograph of a 0.2CNF aerogel on top of a dandelion; (e-h) SEM images of 0.2CNF (e,f) and 0.6CNF (g,h) aerogel pore structures at cross sections, arrow in f indicates thin fibers across the pores; (i) compressive stress-strain (σ - ϵ) curves of 0.2, 0.4 and 0.6CNF aerogels at 2.7, 5.2, and 8.1 mg/cm^3 densities, respectively.

All CNF aerogels are highly porous. The 0.2CNF aerogel contains heterogeneously shaped pores with widely varied sizes from one to few hundred micrometers and encased in smooth thin walls of assembled CNFs (Figure 1e) with traces of fibrils (Figure 1f). The pores become less heterogeneous in shapes and sizes as CNF concentration increases from 0.1 to 0.6% (Figure S3). The pores in 0.6CNF aerogel appear more honey comb shaped and smaller (Figure 1g,h). Irrespective of CNF concentrations, pores in all aerogels appear isotropic along both cross and longitudinal sections and mostly interconnected (Figure S4). The 0.2CNF aerogel has a $10.9 \text{ m}^2/\text{g}$ Brunauer-Emmett-Teller (BET) specific surface and a $0.025 \text{ cm}^3/\text{g}$ cumulative pore volume between $17\text{--}3000 \text{ \AA}$ pore sizes, indicating macroporous or nonporous structure (Figure S5) of the assembled CNFs in the thin walls.

The ultra-light weight and highly porous CNF aerogels remain intact when compressed to 0.8 strain (Figure 1i), impressively ductile and superior to the typically brittle silica aerogels that easily shatter under pressure. The compressive stress-strain curves of all three aerogels show three stages: a linear elastic region at low strain, a non-linear plastic deformation plateau beyond the yield point at

medium strain, then a dramatic stress increase at high strain. The Young's modulus and yield strain increase with increased aerogel densities, showing better elastic properties of those with smaller pores or more closely spaced pore walls (Table S1). The Young's modulus and maximum compressive stress at $\epsilon=0.8$ for 0.6CNF aerogel are 54.5 and 25.3 kPa, respectively (Table S1), relatively low due to their ultralow densities and high porosities. Normalized by its density (8.1 mg/cm^3), the specific compressive modulus of 0.6CNF aerogel is $6.7 \text{ MPa}\cdot\text{cm}^3/\text{g}$, much higher than aerogels from clay ($0.25 \text{ MPa}\cdot\text{cm}^3/\text{g}$ at 40 mg/cm^3 density),⁴⁴ cellulose nanowhisker (below $2 \text{ MPa}\cdot\text{cm}^3/\text{g}$ at 10 mg/cm^3 density) and cellulose nanowhisker/clay composite (below $6 \text{ MPa}\cdot\text{cm}^3/\text{g}$ at 69 mg/cm^3 density).⁴⁵ The higher specific compressive modulus of CNF aerogel indicates much stronger inter-CNF hydrogen bonding and entanglements from their much smaller lateral dimension (2 nm vs. 26 nm for nanowhiskers) and higher aspect ratio (hundreds to approaching 1000 vs. 85 for nanowhiskers).⁴⁵ However, aerogel with much higher mechanical performance (specific compressive modulus of $333 \text{ MPa}\cdot\text{cm}^3/\text{g}$) has been reported from chemically crosslinked graphene oxide aerogel, suggesting crosslinking could potentially improve the mechanical properties of aerogels.⁴⁶ The less dense 0.2CNF aerogel shows only 15% and 7.5% shape recovery at 0.4 and 0.8 strains, respectively (Figure S6), in contrast to the nearly complete shape recovery of



CNT/graphene composite aerogels³¹ and carbonaceous nanofiber aerogels.^{32,33} In air and under the ambient condition, the densest CNF aerogels have higher specific compressive modulus than clay and cellulose nanowhisker aerogels, but inferior compressive elasticity to those of CNT/graphene aerogels.

Figure 2. Water saturated CNF aerogels: (a) water and chloroform absorption capacity as a function of CNF density, dash line represents calculated values from $(\text{porosity}/\rho_{\text{aerogel}})$ at constant volumes; (b) cyclic water and 0.9% NaCl absorption of 0.3CNF (4.0 mg/cm^3) and 0.6CNF aerogels (8.1 mg/cm^3); (c) photographs of 0.2CNF aerogel (2.7 mg/cm^3) compression tested under water, showing initial at $\epsilon = 0$, compressed at $\epsilon = 0.8$ and fully recovered at $\epsilon = 0$ again; (d) compressive stress-strain hysteresis of 0.2CNF aerogel under water at $\epsilon = 0.4$, 0.6, and 0.8; (e) cyclic compressive stress-strain hysteresis of 0.2CNF aerogel under water at $\epsilon=0.6$.

These highly porous CNF aerogels have superior water absorption capacities ranging from $116\text{--}210 \text{ mL/g}$ (or g/g), highest for the 0.3CNF aerogel (4.0 mg/cm^3 density) (Figure 2a). Remarkably, even with over 100 times of their own weights, all water-saturated aerogels retain the same dimensions as in their dry state, showing the absorbed water to be primarily within the macropores. The calculated water absorption capacities based on constant volume

COMMUNICATION

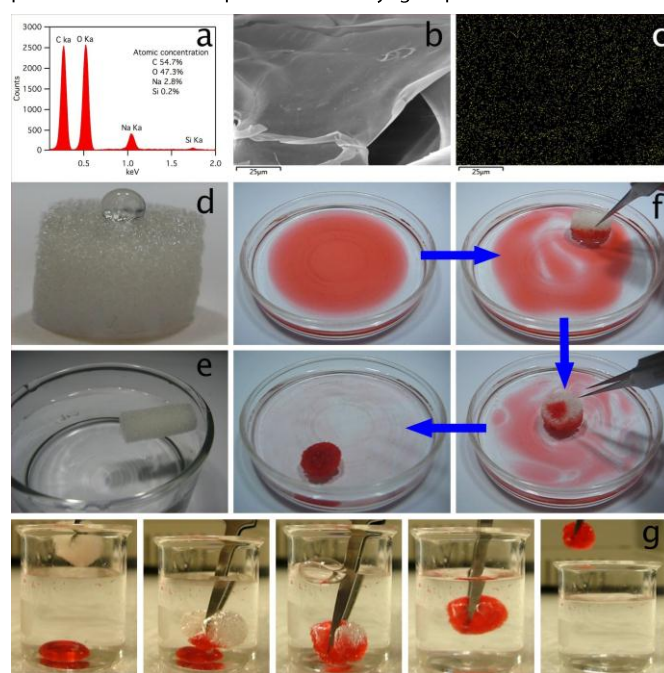
are significantly higher than the measured values for aerogels with densities below 4.0 mg/cm^3 (Figure 2a) and are attributed to the inability of the less dense aerogels to hold water when removed from water. The calculated water absorption values are deemed appropriate for all CNF aerogels while immersed in water and close to the measured values for those with densities at and higher than 4.0 mg/cm^3 . The proportions of measured to calculated absorbency are 25, 46, 83, 91, 91 and 94% for aerogels with increasing densities of 1.7, 2.7, 4.0, 5.2, 6.3 and 8.1 mg/cm^3 , respectively. Denser aerogels have thicker pore walls and smaller pores, more capable of holding the absorbed water when removed from water. In aerogels denser than 4.0 mg/cm^3 , ca. 91 to 94% pores are filled with water, leaving only a few percent of pore volume to be inaccessible to water.

Irrespective of their densities or ability to hold the absorbed water in air, the absorbed water could be easily squeezed out by hand and the squeezed aerogel reabsorbs similar or even more water after several squeezing-absorption cycles, showing excellent wet resiliency and repetitive cyclic water absorption-desorption behavior (Figure 2b). More interestingly, the CNF aerogels also show superior absorption toward saline (0.9% NaCl). 0.3CNF aerogel absorbed 194 and 210 g/g of water and saline, respectively, again showing no volume or shape change. The 8% higher absorption of saline than water, even taking its slightly higher density (1.0046 g/cc) into account, is possibly due to ionization of the carboxyls in saline. Most significantly, the superior 210 g/g saline absorption of CNF aerogels far exceeds the most superabsorbent polymers, e.g., 50 g/g of acrylic-based superabsorbent.⁴⁷ Anionic acrylic-based gels achieve super-absorbencies by swelling from electrostatic repulsion among the anionic moieties and the osmotic pressure inside the gel. In contrast, CNF aerogels absorb water primarily through capillary action and physical containment in the ultra-high volume of pores framed by the strongly hydrogen bonded assembled CNFs, thus less affected by the presence of electrolytes. After four squeezing-absorption cycles, the absorbed saline drop to 156 g/g (Figure 2b), possibly due to decreased osmotic pressure from increased sodium ion association with CNF surface carboxylates. Upon washing with copious amount of water to remove the bound sodium ions, this aerogel absorbs 199 g/g saline, almost fully recovers its absorbency.

The fully water saturated CNF aerogel demonstrates outstanding wet strength under water, withstanding over 0.8 compressive strain and recovering completely once the load is released (Figure 2c,d). Compressive stress-strain hysteresis of water saturated 0.2CNF aerogels shows linear elastic region at $\epsilon < 0.2$, followed by densification regions at $\epsilon > 0.2$. At $\epsilon = 0.8$, the maximum wet stress of fully water saturated 0.2CNF is 1.19 kPa , much lower than 8.47 kPa in air. This wet stress is lower than the 12.1 kPa for carbon nanofiber aerogels at the same strain, owing to the lower density (2.7 mg/cm^3) of 0.2CNF aerogel vs. 10.6 mg/cm^3 for the carbon aerogel and their different structures.³³ The unloading curves return to zero at $\epsilon = 0$ at all three strains, showing complete shape recovery even at high strains. Most impressively, cyclic compression of 0.2CNF hydrogel at $\epsilon = 0.6$ shows complete recovery at up to 100 cycles (Figure 2e), indicating the assembled CNF macroporous structures

are strong to withstand cyclic compression under water. Most strikingly, CNF aerogel remains at the same size after 100 cycles, whereas the carbon nanofiber aerogels showed 11.5% reduction in thickness after 100 cycles.³³ The excellent wet size retention of CNF aerogel could be attributed to its superior hydrophilicity and water absorbency.

With three hydrophilic hydroxyls surrounding each hydrophobic pyranose, each anhydroglucose or cellulose is amphiphilic and should exhibit affinity towards both polar and non-polar liquids. In deed, 0.3CNF aerogel absorbed 144 g/g or 197 mL/g decane, confirming dual polar and non-polar absorbing characteristics, or amphiphilicity. The absorption of decane is 6% lower than that of water (210 mL/g), filling 78% and 83% of the pores, respectively, based on calculated 253 mL/g pore volume for 0.3CNF aerogel. The 0.3CNF aerogel also absorbs 192 mL/g non-polar chloroform or 76% of its total pore volume, comparable to the non-polar decane. In essence, CNF aerogels demonstrate exceptional amphiphilic characteristics with 83% and 78% of total pores could be accessed and filled by polar and nonpolar liquids, respectively. This slightly higher absorption of the highly polar water than the non-polar decane and chloroform suggests this amphiphilic CNF aerogel to be slightly more hydrophilic than oleophilic, consistent with the presence of the more polar C6 carboxyl groups in addition to the C2



and C3 hydroxyls on the CNF surfaces.

Figure 3. Triethoxyl(octyl) silane modified 0.2CNF aerogel: (a) EDS spectrum; (b) SEM image; (c) silicon mapping; (d) photograph of water droplet on top; (e) photograph of floating on water surface without absorption; sequential snapshots of removing (f) a layer of Sudan IV dyed decane on top of water and (g) Sudan IV dyed chloroform at the bottom of water.

Aerogels with varied densities or porosities absorbed 128 to 375 g/g chloroform (or $86\text{--}253 \text{ mL/g}$), i.e., 251 g/g (179 mL/g), 375 g/g (253 mL/g), 284 g/g (192 mL/g), 177 g/g (120 mL/g), 136 g/g (92

Journal of
Materials Chemistry A

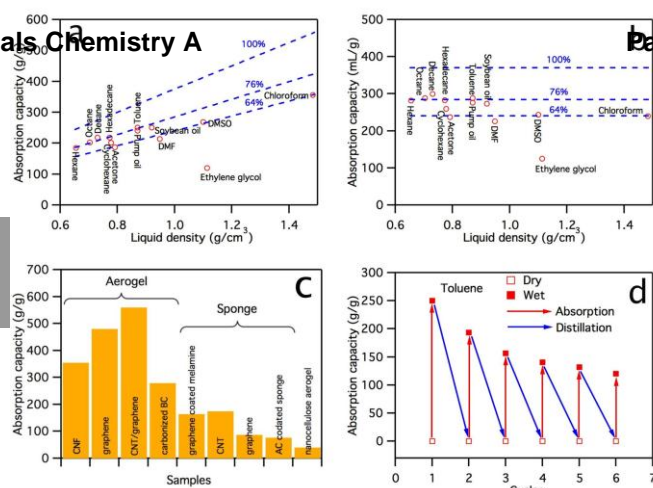
COMMUNICATION

mL/g), 128 g/g (86 mL/g) for 0.1, 0.2, 0.3, 0.4, 0.5 and 0.6 CNF aerogels, respectively (Figure 2a), filling ca. 30, 67, 76, 63, 58 and 70 % of their pore volumes. Chloroform absorption peaked at 375 g/g for the less dense 0.2CNF aerogel whereas peak water absorption was observed on 0.3CNF aerogel. In fact, the aerogel with 4 mg/cm³ density absorbs water and chloroform similarly (ca. 200 mL/g). As noted earlier, less dense aerogels (< 4 mg/cm³) may not retain all the absorbed liquids.

To gain absorption selectivity toward non-polar liquids from the highly polar water, 0.2CNF aerogel was modified by exposure to triethoxyl(octyl) silane vapor at 120 °C for 12 h under vacuum to reduce its surface hydrophilicity (Figure S7) without altering its pore structure and surfaces (Figure S8). Energy dispersive X-ray spectroscopy (EDS) of organosilane vapor deposited aerogel shows a small Si K α peak at 1.74 keV at a 0.2 at%, confirming the presence of Si (Figure 3a). The silane-modified 0.2 CNF aerogel shows uniformly Si covered surfaces (Figure 3b,c) and becomes completely non-wettable by water as shown by water droplet beading up and staying afloat on water surface (Figure 3d,e). This is in contrast to the original aerogel that is instantaneously wetted by water, rapidly water-absorbing and completely submerges under water surface (Figure S9). The hydrophobic silane-modified CNF aerogel rapidly absorbs Sudan IV red dyed decane spread on water, completely removing it within two minutes and leaving clear water (Figure 3f). Besides, the aerogel demonstrated apparent absorption selectivity toward organic solvent than water by selectively removing chloroform from the bottom of water (Figure 3g, Movie S2). The ability to rapidly and completely absorb a hydrocarbon from water demonstrates the excellent oil removal capability of the silane-modified CNF aerogel. Yet, when forced under water, the silane-modified aerogel could still absorb 11.4 g/g water, significantly less than the 173.6 g/g of unmodified aerogel.

Figure 4. Absorption capacity of silane-modified 0.2CNF aerogels: (a) mass based (g liquid per g of aerogel); (b) volume based (mL liquid per g of aerogel) with dash lines representing 100%, 76% and 64% absorption capacities calculated from $(\text{porosity} \times \rho_{\text{liquid}} / \rho_{\text{aerogel}})$ in (a) and $(\text{porosity} / \rho_{\text{aerogel}})$ in (b); (c) chloroform absorption capacity in comparison with graphene aerogel,²⁸ CNT/graphene aerogel,³¹ carbonized bacterial cellulose (BC) aerogel,³² graphene coated melamine sponge,²⁹ CNT sponge,²⁷ graphene sponge,³⁰ activated carbon (AC) coated sponge,⁴⁸ nanocellulose aerogel;²⁰ (d) cyclic absorption and distillation of toluene.

Furthermore, this silane-modified 0.2CNF aerogel exhibits excellent absorption capacities, ranging from 139 to 356 g/g, toward a wide range of non-polar liquids, including various aliphatic (hexane, octane, decane, hexadecane), cyclic (cyclohexane) and aromatic (toluene) hydrocarbons and oils (pump, soybean) (Figure 4a). The volume based absorption capacities of the silane-modified 0.2CNF aerogel toward all non-polar liquids are similar, around 280 mL/g (Figure 4b), ca. 76% of the calculated pore volume for 0.2CNF aerogel (Figure 4a,b), indicating similar hydrophobic interaction with all non-polar liquids. The 24% unfilled pores are thought to be either un-accessible to the liquids and/or occupied by trapped air. When submerged under decane in vacuum, bubbles are observed releasing from the aerogel, indicating some trapped air to impede



liquid to get in. However, the absorption capacity under vacuum decreases by ca. 10%, possibly due to overall volume contraction (around 6%). The hydrophobic silane-modified 0.2CNF aerogel also exhibits descent absorption capacity toward polar aprotic solvents, i.e., acetone at 187 g/g (236 mL/g), DMF at 214 g/g (226 mL/g) and DMSO at 268 g/g (244 mL/g). The absorption capacities towards all polar aprotic solvents are around 64% of the calculated pore volume, slightly lower than the 76% toward non-polar hydrocarbons, again consist with the increased hydrophobicity of the silane-modified aerogels. The much lower absorption capacity toward polar ethylene glycol (139 g/g or 125 mL/g) is ascribed mostly to the hydrophobicity of silane-modified aerogel and high viscosity of the liquid.

The original 0.2CNF aerogels absorbed similar amount of chloroform and decane (375 and 195 g/g, respectively) as the silane-modified (356, and 219 g/g, respectively), consistent with the amphiphilic nature of the unmodified aerogels. Silanization converts some hydrophilic surfaces to hydrophobic, slightly improved decane absorption. Most significantly, partial hydrophilicity-to-hydrophobicity conversion causes silane-modified CNF aerogels to become non-wettable by water and not water-absorbing, affording excellent preferential absorption of non-polar liquids over water. In general, the absorption capacities of silane-modified 0.2CNF aerogel toward non-polar hydrocarbons and oils are from ca. 200 g/g to 350 g/g, i.e., one order of magnitude higher than previously reported values for cellulose aerogels (20-40 times),²⁰ and at least 2-3 times greater than CNT sponge (80-180 times),²⁷ carbonaceous aerogels (40-120 times),³³ graphene sponges (54-165 times),²⁹ mesoporous graphene (up to 66 times)⁴⁹ and activated carbon coated sponges (27-86 times).⁴⁸ It should also be noted that these CNF aerogels derived from rice straw cellulose absorbed 240 g/g of pump oil, far superior to acetylated rice straw (17-24 g/g of machine oil).¹⁴ The absorption capacity of CNF aerogel toward chloroform was further compared with other superabsorbents, showing much higher absorbency than all aerogels except for graphene²⁸ and CNT/graphene³¹ aerogels (Figure 4c). The reported graphene-based aerogels require complicated, costly and energy-intensive processes (Table S2). In contrast, these rice straw CNF aerogels are derived from abundant under-utilized agricultural crop by-product via aqueous processing with considerably less chemical and energy input, making them particularly attractive materials for oil removal.

In all cases, the absorbed liquids could be easily distilled for collection and recovery (Figure 4d and Figure S10). Upon six absorption-distillation cycles and solvent evaporation, these aerogels appear slightly smaller in dimensions and have lower absorption capacities for octane (125 g/g), cyclohexane (116 g/g) and toluene (120 g/g) or 61, 57 and 48 % of their initial absorption capacities, respectively. The substantial retention of hydrocarbon absorbent capacities after six absorption-distillation cycles indicates very good recyclability of these CNF aerogels for oil absorption.

COMMUNICATION

In summary, novel ultra lightweight (as low as 1.7 mg/cm³), highly porous (as high as 99.9%) CNF aerogels have been successfully fabricated from rice straw cellulose. The 1-2 nm wide and micrometer long CNFs derived from coupled TEMPO oxidation and mechanical blending assemble into monolithic forms of porous structures through facile freezing (-20 °C) and freeze-drying (-50 °C, 0.05 mbar, 2 days) processes. These CNF aerogels show superior wet compressibility and complete shape recovery in water up to 100 cycles. These CNF aerogels are amphiphilic, showing superior absorbency towards both water (210 g/g) and non-polar chloroform (375 g/g). These CNF aerogels also exhibit extraordinary absorption of over 200 times toward saline solution (0.9 wt% NaCl), far exceeding acrylic-based superabsorbents. The hydrophobicity of CNF aerogels could be further enhanced via simple chemical vapor deposition of (triethoxyl(octyl) silane) to absorb 139-356 times organic solvents or oils by weight, far superior than all absorbents derived from natural organic, inorganic or synthetic polymers and approaching the best performing CNT and graphene aerogels.

Notes and reference

Fiber and Polymer Science, University of California, Davis, CA95616, USA

E-mail: ylhsieh@ucdavis.edu; Fax: +1 530 752 7584; Tel. +1 530 752 0843

† Electronic Supplementary Information (ESI) available: CNF isolation and aerogel characterization, pictures and SEM images, BET isotherm and pore distribution, mechanical properties, silanization, comparison with other carbon and bio-based aerogels, cyclic absorption and video clips showing the aerogel "fly" due to static electricity. See DOI: 10.1039/b000000x/

- N. P. Ventikos, E. Vergetis, H. N. Psaraftis and G. Triantafyllou, *Journal of Hazardous Materials*, 2004, **107**, 51-58.
- J. K. Yuan, X. G. Liu, O. Akbulut, J. Q. Hu, S. L. Suib, J. Kong and F. Stellacci, *Nature Nanotechnology*, 2008, **3**, 332-336.
- R. M. Atlas, *International Biodeterioration & Biodegradation*, 1995, **35**, 317-327.
- R. R. Lessard and G. Demarco, *Spill Science & Technology Bulletin*, 2000, **6**, 59-68.
- C. Teas, S. Kalligeros, F. Zankos, S. Stournas, E. Lois and G. Anastopoulos, *Desalination*, 2001, **140**, 259-264.
- J. G. Reynolds, P. R. Coronado and L. W. Hrubesh, *Energy Sources*, 2001, **23**, 831-843.
- O. Carmody, R. Frost, Y. F. Xi and S. Kokot, *Journal of Colloid and Interface Science*, 2007, **305**, 17-24.
- M. Inagaki, A. Kawahara, Y. Nishi and N. Iwashita, *Carbon*, 2002, **40**, 1487-1492.
- Q. F. Wei, R. R. Mather, A. F. Fotheringham and R. D. Yang, *Marine Pollution Bulletin*, 2003, **46**, 780-783.
- Y. L. Zhang, S. Wei, F. J. Liu, Y. C. Du, S. Liu, Y. Y. Ji, T. Yokoi, T. Tatsumi and F. S. Xiao, *Nano Today*, 2009, **4**, 135-142.
- A. Li, H. X. Sun, D. Z. Tan, W. J. Fan, S. H. Wen, X. J. Qing, G. X. Li, S. Y. Li and W. Q. Deng, *Energy & Environmental Science*, 2011, **4**, 2062-2065.
- X. S. Wang, J. Liu, J. M. Bonfont, D. Q. Yuan, P. K. Thallapally and S. Q. Ma, *Chemical Communications*, 2013, **49**, 1533-1535.
- G. Deschamps, H. Caruel, M. E. Borredon, C. Bonnin and C. Vignoles, *Environmental Science & Technology*, 2003, **37**, 1013-1015.
- X. F. Sun, R. C. Sun and J. X. Sun, *Journal of Agricultural and Food Chemistry*, 2002, **50**, 6428-6433.
- H. M. Choi and R. M. Cloud, *Environmental Science & Technology*, 1992, **26**, 772-776.
- T. T. Lim and X. F. Huang, *Chemosphere*, 2007, **66**, 955-963.
- M. Paakko, J. Vapaavuori, R. Silvennoinen, H. Kosonen, M. Ankerfors, T. Lindstrom, L. A. Berglund and O. Ikkala, *Soft Matter*, 2008, **4**, 2492-2499.
- T. Saito, T. Uematsu, S. Kimura, T. Enomae and A. Isogai, *Soft Matter*, 2011, **7**, 8804-8809.
- M. Kettunen, R. J. Silvennoinen, N. Houbenov, A. Nykanen, J. Ruokolainen, J. Sainio, V. Pore, M. Kemell, M. Ankerfors, T. Lindstrom, M. Ritala, R. H. A. Ras and O. Ikkala, *Advanced Functional Materials*, 2011, **21**, 510-517.
- J. T. Korhonen, M. Kettunen, R. H. A. Ras and O. Ikkala, *ACS Applied Materials & Interfaces*, 2011, **3**, 1813-1816.
- N. T. Cervin, C. Aulin, P. T. Larsson and L. Wagberg, *Cellulose*, 2012, **19**, 401-410.
- H. W. Liang, J. W. Liu, H. S. Qian and S. H. Yu, *Accounts of Chemical Research*, 2013, **46**, 1450-1461.
- J. W. Liu, H. W. Liang and S. H. Yu, *Chemical Reviews*, 2012, **112**, 4770-4799.
- Y. Habibi, L. A. Lucia and O. J. Rojas, *Chemical Reviews*, 2010, **110**, 3479-3500.
- L. B. Hu, G. Y. Zheng, J. Yao, N. A. Liu, B. Weil, M. Eskinsson, E. Karabulut, Z. C. Ruan, S. H. Fan, J. T. Bloking, M. D. McGehee, L. Wagberg and Y. Cui, *Energy & Environmental Science*, 2013, **6**, 513-518.
- F. Jiang and Y.-L. Hsieh, *Journal of Materials Chemistry A*, 2014, **2**, 350-359.
- X. C. Gui, J. Q. Wei, K. L. Wang, A. Y. Cao, H. W. Zhu, Y. Jia, Q. K. Shu and D. H. Wu, *Advanced Materials*, 2010, **22**, 617-621.
- Y. Zhao, C. G. Hu, Y. Hu, H. H. Cheng, G. Q. Shi and L. T. Qu, *Angewandte Chemie-International Edition*, 2012, **51**, 11371-11375.

COMMUNICATION

29. D. D. Nguyen, N. H. Tai, S. B. Lee and W. S. Kuo, *Energy & Environmental Science*, 2012, **5**, 7908-7912.
30. H. C. Bi, X. Xie, K. B. Yin, Y. L. Zhou, S. Wan, L. B. He, F. Xu, F. Banhart, L. T. Sun and R. S. Ruoff, *Advanced Functional Materials*, 2012, **22**, 4421-4425.
31. H. Sun, Z. Xu and C. Gao, *Advanced Materials*, 2013, **25**, 2554-2560.
32. Z. Y. Wu, C. Li, H. W. Liang, J. F. Chen and S. H. Yu, *Angewandte Chemie-International Edition*, 2013, **52**, 2925-2929.
33. H. W. Liang, Q. F. Guan, L. F. Chen, Z. Zhu, W. J. Zhang and S. H. Yu, *Angewandte Chemie-International Edition*, 2012, **51**, 5101-5105.
34. W. G. Glasser, R. H. Atalla, J. Blackwell, R. M. Brown, W. Burchard, A. D. French, D. O. Klemm and Y. Nishiyama, *Cellulose*, 2012, **19**, 589-598.
35. I. Kalashnikova, H. Bizot, B. Cathala and I. Capron, *Biomacromolecules*, 2012, **13**, 267-275.
36. J. P. Zhang and S. Seeger, *ChemPhysChem*, 2013, **14**, 1646-1651.
37. W. S. Chen, H. P. Yu, Q. Li, Y. X. Liu and J. Li, *Soft Matter*, 2011, **7**, 10360-10368.
38. W. Zhang, Y. Zhang, C. H. Lu and Y. L. Deng, *Journal of Materials Chemistry*, 2012, **22**, 11642-11650.
39. P. Lu and Y. L. Hsieh, *Carbohydrate Polymers*, 2012, **87**, 564-573.
40. F. Jiang, S. Han and Y.-L. Hsieh, *RSC Advance*, 2013, **3**, 12366-12375.
41. H. Sehaqui, M. Salajkova, Q. Zhou and L. A. Berglund, *Soft Matter*, 2010, **6**, 1824-1832.
42. T. M. Tillotson and L. W. Hrubesh, *Journal of Non-Crystalline Solids*, 1992, **145**, 44-50.
43. J. H. Zou, J. H. Liu, A. S. Karakoti, A. Kumar, D. Joung, Q. A. Li, S. I. Khondaker, S. Seal and L. Zhai, *Acs Nano*, 2010, **4**, 7293-7302.
44. M. D. Gawryla, M. Nezamzadeh and D. A. Schiraldi, *Green Chemistry*, 2008, **10**, 1078-1081.
45. M. D. Gawryla, O. van den Berg, C. Weder and D. A. Schiraldi, *Journal of Materials Chemistry*, 2009, **19**, 2118-2124.
46. H. Huang, P. Chen, X. Zhang, Y. Lu and W. Zhan, *Small*, 2013, **9**, 1397-1404.
47. K. Kabiri, H. Omidian, S. A. Hashemi and M. J. Zohuriaan-Mehr, *European Polymer Journal*, 2003, **39**, 1341-1348.
48. H. X. Sun, A. Li, Z. Q. Zhu, W. D. Liang, X. H. Zhao, P. Q. La and W. Q. Deng, *Chemsuschem*, 2013, **6**, 1057-1062.
49. Z.-L. Fan, X.-J. Qin, H.-X. Sun, Z.-Q. Zhu, C.-j. Pei, W.-D. Liang, X.-M. Bao, J. An, P.-Q. La, A. Li and W.-Q. Deng, *Chempluschem*, 2013, **78**, 1282-1287.

